MICROMACHINED STIMULATING ELECTRODES

Quarterly Report #4

(Contract NIH-NINDS-N01-NS-2-2379)

July --- September 1993

Submitted to the

Neural Prosthesis Program
National Institute of Neurological Disorders and Stroke
National Institutes of Health

by the

Solid-State Electronics Laboratory
Bioelectrical Sciences Laboratory
Department of Electrical Engineering and Computer Science
University of Michigan
Ann Arbor, Michigan
48109-2122

December 1993

MICROMACHINED STIMULATING ELECTRODES

Summary

During the past quarter, research under this program has gone forward in a number of areas. Passive probe fabrication has continued with the fabrication of several runs of "EMORY" probes. A set of "HMRI" probes are also ready for metal. Problems with our iridium target, which separated from its backing plate recently, have been fixed and a backup iridium target has been ordered to avoid any problems in the future. Probes for studies of tissue penetration, aimed at quantifying the insertion force required for pia arachnoid and dura mater as a function of tip shape, are nearing completion along with a workstation-based system for data acquisition and analysis. These probes feature a wide range of tip angles and shapes, fabricated both with single- and with double-diffused processing. Initial tests of these probes are expected during the coming term. Studies of chronic stimulating electrode impedance and tissue access voltage are underway as well, and while only preliminary results are available at this writing, impedances have been observed to generally increase during stimulation but to decline over time between stimulation sessions. The access voltage drops significantly after several days of stimulation. These studies are continuing and more conclusive results should be available during the coming quarter.

A fabrication run of second-generation active stimulating probes has been completed through circuit metallization. Test results have shown small deviations in the threshold voltages from the design targets and a low poly-gate field transistor threshold; however, transistor leakage currents are nonetheless submicroampere over the expected operating range of the circuitry. Significant leakage problems associated with earlier active probes have been eliminated by using wider p-well-to-p-well separations and a wider epitaxial layer. Tests have shown that all of the STIM-1B (monopolar), STIM-1A (bipolar), and STIM-2 (8 of 64 parallel) circuit blocks are fully functional, with performance near design targets. This includes the functions of power-on-reset, internal clock generation, data input, data latching, channel selection, level shifting, and digital-to-analog conversion. These probes are now being completed with the application of LTO over the circuit areas, the addition of iridium at the sites, and the use of micromachining to free them from the wafer. We hope to have fully functional probes during the coming quarter.

MICROMACHINED STIMULATING ELECTRODES

1. Introduction

The goal of this research is the development of active multichannel arrays of stimulating electrodes suitable for studies of neural information processing at the cellular level and for a variety of closed-loop neural prostheses. The probes should be able to enter neural tissue with minimal disturbance to the neural networks there and deliver highly-controlled (spatially and temporally) charge waveforms to the tissue on a chronic basis. The probes consist of several thin-film conductors supported on a micromachined silicon substrate and insulated from it and from the surrounding electrolyte by silicon dioxide and silicon nitride dielectric films. The stimulating sites are activated iridium, defined photolithographically using a lift-off process. Passive probes having a variety of site sizes and shank configurations have been fabricated successfully and distributed to a number of research organizations nationally for evaluation in many different research preparations. For chronic use, the biggest problem associated with these passive probes concerns their leads, which must interface the probe to the outside world. Even using silicon-substrate ribbon cables, the number of allowable interconnects is necessarily limited, and yet a great many stimulating sites are ultimately desirable in order to achieve high spatial localization of the stimulus currents.

The integration of signal processing electronics on the rear of the probe substrate (creating an "active" probe) allows the use of serial digital input data which can be demultiplexed onto the probe to provide access to a large number of stimulating sites. Our goal in this area of the program has been to develop a family of 16-site active probes capable of chronic implantation in tissue. For such probes, the digital input data must be translated on the probe into per-channel current amplitudes which are then applied to the tissue through the sites. Such probes require five external leads, virtually independent of the number of sites used. As discussed in our previous reports, we have defined three probes which represent the first-generation of these active stimulating devices and have designated them as STIM-1, -1A, and -1B. All three probes provide 8-bit resolution in setting the per-channel current amplitudes over the biphasic range from 2μA to ±254μA; however, the probes differ markedly in the number of sites that can be active at any one time. STIM-1 offers the ability to utilize all 16 sites independently and in parallel, while -1A allows only two sites to be active at a time (bipolar operation), and -1B is a monopolar probe, allowing the user to guide an externally-provided current to the site selected by the digital address. The circuit complexity among these designs spans an order of magnitude in device count, ranging from a 400 transistors (STIM-1B) to over 7000 transistors (STIM-1). The high-end STIM-1 contains provisions for numerous saftey checks and for features such as remote impedance testing in addition to its normal operating modes.

During the past quarter, research on this contract has focused in four areas. Several runs of passive probes have been fabricated, and probes are continuing to be distributed to a variety of external users. Probes for studies of tissue penetration as a function of tip shape are nearly completed and instrumentation for these experiments is being readied. In addition, studies of chronic site impedance and tissue access resistance under conditions of periodic stimulation have been started. A fabrication run of first- and second-generation active probes has been completed through circuit metal and found to be fully functional

with performance close to design targets. These include versions of STIM-1B, and STIM-1A and well as both 8 and 16-shank versions of STIM-2. Prototype versions of the low-profile version of STIM-2 have been etched out and found to exhibit adequate micromachining yield and the ability to be formed so that the circuitry lays flat against the cortex to mainitain a very low implant profile. The activities in these areas are described in the sections below.

2. *Passive Stimulating Electrode Development*

During the past quarter, two new masks were obtained for the existing "EMORY" mask set. This mask set includes stimulating and recording electrode designs for both internal and external users. The new masks permit us to metalize the sites and bonding pads separately (iridium sites, gold pads) so that bonding to the pads will be easier, particularly for external users. Aluminum wire can be bonded to iridium but several external users have found it virtually impossible to bond to it with gold wire. The first wafers completed using these new masks appeared to have an interfacial oxide present at the sites due to incomplete removal of the upper oxide layer over the polysilicon interconnects. This residual oxide layer could be eliminated (broken down) by applying a DC voltage (15-20V) across the site with respect to a platinum reference in saline. A 1-10Megohm resistor was placed in series with the site to provide current limiting. After being "repaired", the sites demonstrated normal to below-normal impedances and appeared to activate normally. After these probes were characterized, a new fabrication run of "EMORY" probes was also completed. Most of the wafers from this run were free from interfacial oxide problems and are being distributed to users; one or two wafers appeared to have some low-current rectification at the sites (probably due to interfacial oxide), although it could be broken down at applied voltages below 2V. A fabrication run of "HMRI" probes has also now been completed up to iridium deposition, and probes from this group of wafers should be available within the coming month.

2.1 *Penetration Studies*

As discussed in previous quarterly reports, a series of probes has been designed to study the insertion forces, long-term probe-tissue coupling, and tissue damage associated with penetration through the pia arachnoid and dura mater in guinea pigs, rats and perhaps primates. These probes will be used to determine the optimal probe shank geometry which allows for ease of penetration with minimal cortical surface dimpling, minimal tissue damage and reaction along the insertion track, and maximal tissue-electrode coupling.

During the past quarter, the development of a data acquisition system which will be used to collect the results associated with these penetration experiments has continued. We plan to collect data on probe stress/insertion force as a function of position and to optically view the insertion process to determine the spatial depression of the cortex prior to penetration. Several LabView routines are being developed to allow acquisition of the data by computer, and a custom hardware interface is now being completed to allow position and strain data to be collected along with sample video frames. In previous work at the Kresge Hearing Research Institute (KHRI), a problem was encountered involving the mechanical stability of our probe advance system. While performing probe penetrations with devices used in previous acute experiments, a significant amount of lateral movement (perpendicular to the direction of penetration) was observed. This movement is undesirable because it complicates tissue penetration and induces unnecessary trauma to the tissue. Any lateral movement also reduces the effectiveness of video capture. This problem is

greatly magnified if the microscope with the video mount vibrates as well, causing frame-to-frame misalignment. Difficulties with the analysis of the image data are then compounded. Finally, any lateral movement during penetration will cause deflection of the probe shanks, introducing noise into the strain gauge readings. Solving this problem is important not only in these penetration experiments but in any probe implant because of the tissue damage it can cause.

Most of the undesirable probe movement was found to be the result of vibration translated into the system from outside sources. There will inevitably be a certain amount of vibration from mechanical movement of the microdrive system as well. In order to minimize outside sources of movement, we have updated the shock absorbers of the work table at KHRI and are looking into ways of minimizing vibration in the microdrive system. Instead of mounting the microdrive on a long-armed support, which effectively amplifies any vibration, we have gone to a shorter and more rigid mounting system. A new light-weight microdrive has also been purchased that offers better control than our older unit along with a direct interface to the computer for position monitoring and control.

Another potential problem is also being explored in connection with strain gauge calibration and measurement methods being developed. We have based our approach on work done previously here by Najafi and Hetke (*IEEE Trans. Bio. Engr.*, 37, pp. 474-481, 1990), who characterized the strength of silicon microprobes using on-chip polysilicon strain gauges. Their associated theoretical calculations assumed that the probe makes a normal approach to the tissue surface. Inevitably, there will be at least a slight off-normal approach angle, which will contribute a non-axial force component along the probe shank (Fig. 1). This will cause the probe shank to buckle more easily and will introduce error into the strain gauge measurements. Prior to buckling, the strain gauge measures only the axial compression of the shank, but when the shank begins to buckle, the curvature of the shank introduces a different compression/tension on the strain gauge depending on whether it is located on the inside or outside surface of the shank relative to its curvature. The question is then how much off-axis angle is allowable in the probe shank orientation before it will significantly alter the characterization measurements. We are currently doing theoretical calculations to answer to these questions.

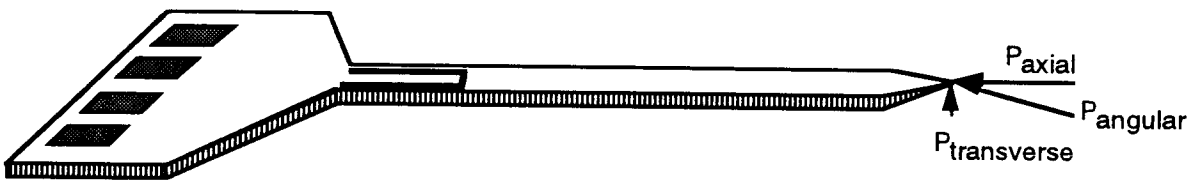

Fig. 1: Force components in a non-perpendicular approach to the cortical surface.

The fabrication of a set of probes for use in these penetration studies was delayed during the past quarter due to a number of equipment problems in the fabracation facility. These involved problems with our four-inch boron diffusions, with the LPCVD nitride/oxide deposition reactor, and with the iridium sputtering target. The first two problems were corrected with a minimum of delay; however, the iridium source problem was potentially more serious. The iridium target came unbonded from the heavy backing plate to which it is fixed, probably due to stress in the iridium. This is the second time this has occurred, and initially we feared that it could not be corrected. New iridium targets are

fabricated as needed with a delay of at least 8-10 weeks. Fortunately, the target has now been repaired and the penetration probes should be completed within a few weeks. A back-up sputtering target has also been ordered to protect against any future downtime if the target separates again and cannot be repaired.

During the coming quarter we expect to complete fabrication of the penetration probes, which include both single- and double-diffused tips as well as a variety of tip angles. We also expect to finish the development of the data acquisition system and to perform initial experiments to quantify the effect of tip shape on the ease with which pia arachnoid and dura mater can be penetrated.

2.2 In-Vivo Current Flow and Impedance Studies

Investigations into the current flow and impedance of passive stimulating probes in-vivo are progressing. This past quarter was spent finishing the development of a test system that will be used for electrode testing *in-vivo* and *in-vitro*. One experiment has been completed. In addition, equipment for an electrode activation and characterization system has been purchased and received. The CFos experiment discussed in the last quarterly report has been postponed while our methods are investigated and refined.

The first stimulation experiment was recently completed on a chronically-implanted guinea pig. The probe used was the three-shank six-site structure with a silicon cable described in previous reports. The probe has two 1000μm^2 iridium sites per shank. The animal was stimulated between sites on the same shank and between sites on different shanks, and measurements of access voltage and site-to-site impedance were taken. It is theorized that as tissue reaction occurs, differences will develop in these parameters.

The animal preparation was different than the one described in previous reports. We had hoped to implant in the cochlear nucleus, but due to difficulties that will be discussed later, our present approach is to implant in visual cortex. An adult guinea pig, approximately 460 gm, was anesthetized with 0.4cc of 1:1 Ketamine:Rompan. The skull was exposed and four small screws were inserted in a square pattern at the top of the skull. A larger machine screw (the head screw) was placed inverted inside the square and secured to the small screws with dental acrylic. After the acrylic hardened, the animal's head was immobilized by attaching the head screw to a rigid bar.

A small hole was made (with a dental drill) above the right visual cortex. The dura was cut to expose the cortex. The probe connector was attached to the skull with dental acrylic. The probe was grasped with a suction tool and inserted into the cortex. The skull defect was filled with agar and covered with dental acrylic. Dental acrylic was agin used to secure the connector to the head screw area, forming a stable implant site capable of withstanding cage life. The animal was given 0.25cc of chloromycetin as a profillactic against infection and 0.1cc of dexamethasone to reduce inflammation. The animal was allowed to recover for a period of six days before the stimulation and measurements of the experiment began.

The test system used is a 486 PC running the data acquisition software LabVIEW (National Instruments). LabVIEW drives an analog input/output board to present stimuli and record data. A voltage signal is fed from the computer to a proportional current driver. The current source is connected to a computer-controlled relay system (Matrix Systems) which routes the stimulus to the desired site. The entire test is run under computer control.

LabVIEW has been programmed to automatically collect data and change stimulation sites at intervals predetermined by the user.

The stimulation protocol is 50μA of biphasic stimulation for four hours on each site pair. Site pairs 5-6 and 2-3 were used. Sites 5 and 6 are on one shank and sites 2 and 3 are on different shanks. The animal is placed in an enclosure and is connected to the system via a swivel connector. This allows for free movement during the experiment. Measurements of impedance and access voltage were taken before, during, and after the stimulation period. The experiments were run five times in six days. Several data sets were lost in the first animal due to programming errors and the guinea pig chewing through the test leads. In addition, no phase data was obtained during the stimulation. This was also a programming error. A polyurethane catheter was subsequently placed around the test leads to discourage the animal from chewing. The catheter is flexible enough that it does not impede movement. The programming errors have been identified and will be corrected before any further tests are attempted.

Impedance data was collected before and after each stimulation period. A 1kHz sine wave was used to measure impedance. One hundred cycles were collected and averaged. The results are shown in Table 1.

Day	Site Pair , before or after stimulation	Impedance (KOhm)	Phase (deg.)
1	5-6, after	743	28.8
1	2-3, before	342	14.4
1	2-3, after	652	36.0
2	5-6, before	211	21.6
2	5-6, after	987	36.0
3	5-6, before	514	21.6
3	5-6, after	716	21.6
3	2-3, before	94	7.2
5	5-6, before	24	21.6
5	5-6, after	28	21.6
5	2-3, before	37	14.4
6	5-6, before	29	14.4
6	5-6, after	33	14.4
6	2-3, before	25	14.4
6	2-3, after	28	14.4

Table 1: Site-to-Site impedance measurements taken before and after 4 hours of biphasic stimulation at 50μA. The impedance was measured at 1kHz.

Data for access voltage was taken during each four hour stimulation period. Data was automatically collected every 30 minutes. One hundred cycles were collected and averaged. The results are shown in Table 2.

The missing data leaves a few gaps, but some general trends are evident. The impedance increases after the stimulation period but declines during the week. After a day of rest, the impedance magnitude dropped significantly. The most striking result is the drastic reduction in the access voltage and impedance after a number of days of stimulation. This may be due to additional activation of the electrode sites bringing a lower impedance. Another possibility is the presence of a leakage current in the system. The equipment is currently being checked for any leakage paths. Some difference is seen in both impedance

and access voltage for between-shank and along-shank stimulation. Further validation of the test setup and more experimental data are needed to determine if the results presented above are valid. Until consistency is seen across several experiments, we cannot make any conclusions about these experiments. They are seen as a check-out of the experimental procedure and test equipment more than as a data set for interpretation.

Day	Site Pair	Access Voltage (V) at Time Interval (min.)							
		30	60	90	120	150	180	210	240
1	5,6	11.5	11.3	9.6	9.1	16.5	14.1	13.6	13
1	2,3	11.8	13	14.1	14.5	13.8	14	11.1	14.3
2	5,6				8.3	7.7	9	16	16.5
3	5,6	12.1	12.2	12.5	11.3	11.2	11.2	11.9	12
3	2,3	4.2	3.9	4	4.2	4.2	4.3	4.3	4.3
5	5,6	0.9	1.05	1	1.1	1.1	1.1	1.2	1.2
6	5,6	1.6	1.5	1.6	1.6	1.5	1.6	1.6	1.6
6	2,3	1.2	1.3	1.3	1.4	1.4	1.3	1.3	1.4

Table 2: Access voltage for 50μA biphasic stimulation.

Additional work on passive stimulating probes was done in the following areas. We have purchased a system for activation and characterization of electrodes *in vitro*. The equipment includes a 486 PC, LabVIEW software, and two National Instruments I/O cards. Software and external electronics need to be developed for this system. Also, several CFos experiments were attempted. CFos is a protein produced by stimulated neurons. An immunoflourescent label can mark tissue samples and show which neurons were stimulated. We attempted to use CFos marking to show the effectiveness of a stimulating electrode implanted in the cochlear nucleus (CN). However, the cable length on the probes currently being used appears to be too short for these chronic implants. We think this caused the electrode to become dislodged from the CN as the animal grew during its recovery period. This speculation is based on observations made during surgery on a relatively large guinea pig. More cable length is required to allow for growth. We are also investigating methods of securing the electrode by gluing it to the neural tissue. We hope to run experiments this winter to test some of these methods.

3. *Development of Active Stimulating Probes (STIM-2)*

3.1 *Testing of the STIM Probes (STIM1B, STIM1A, STIM2)*

During the past quarter, the fabrication of first- and second-generation active stimulating probes containing CMOS circuitry was completed up to the aluminum metallization step, and the associated circuitry was tested. The results are encouraging with nearly all of the circuitry working as designed. First, we tested all of the individual device characteristics, including the CMOS transistors, field transistors (i.e., test transistors fabricated over field oxide), p-well-to-well punch-through voltages, p-well-to-substrate

punch-through voltages, and sheet resistances. The p-well-to-substrate punch-through voltage is of greatest concern because it caused excessive leakage current in past runs. (This was the source of the "phantom" background currents on STIM-1.) After the completion of device testing, we proceeded to test all of the circuit blocks related to the stimulating circuits. We are now in the process of completing the processing of these active probes through the addition of LTO over the circuit areas, iridium inlays at the sites, and micromachining to perform probe separation from the host wafers.

DEVICE LEVEL TESTS

Figure 2 shows the current-voltage characteristics of typical CMOS devices (p-MOS and n-MOS transistors) from this fabrication run. These devices are working properly as designed. Figure 3 shows the p-well-to-p-well punch-through characteristics for the minimum design rules associated with this process ($6\lambda = 9\mu m$). This test result shows a high electrical immunity to well-to-well punch-through. The leakage at a bias of 26V is less than 80nA. Figure 4 shows the p-well-to-substrate punch-through characteristic, which shows high electrical device isolation up to 26V between the p-well and both the n-epi layer and the p-substrate. The leakage at 26V is again well below $1\mu A$. These improvements reflect the wider separations maintained between p-wells and the thicker epi layers used for this run of probes.

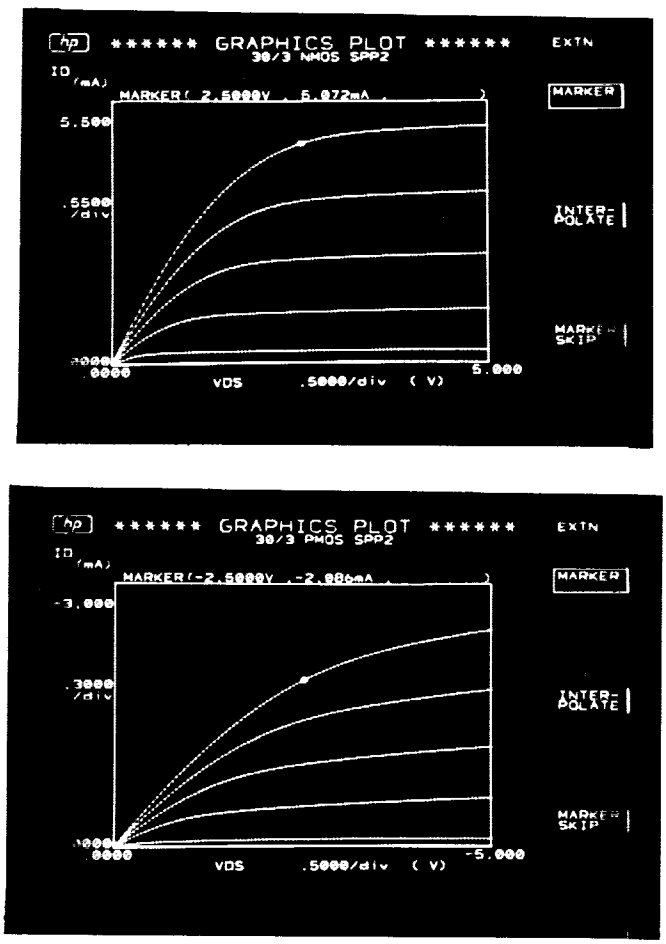

Fig. 2: Measured CMOS device characteristics; (a) n-MOS and (b) p-MOS transistors. The gate voltage ($|V_{GS}|$) step is 1.0V with a total range of 1.0V to 5.0V.

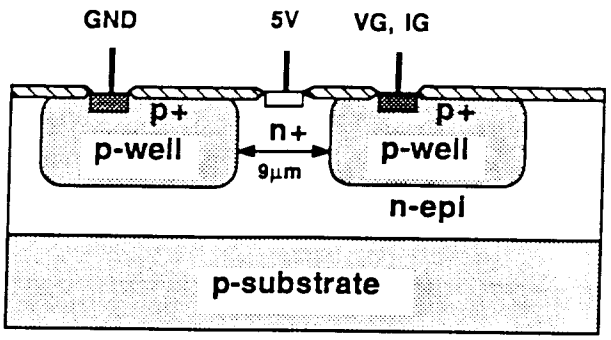

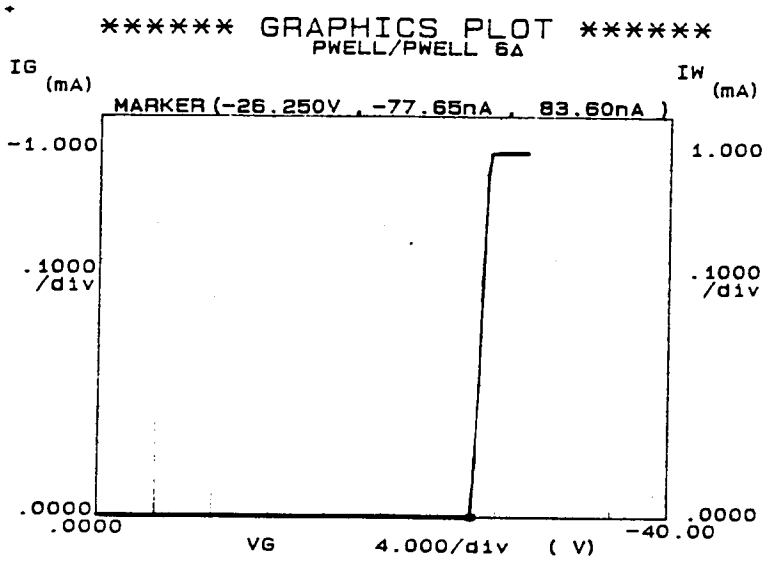

Fig. 3: Measured p-well-to-p-well punch-through characteristics. One of p-wells is biased to ground, the n-epi layer is biased at Vcc (5V), and the other p-well is swept 0V to -30V.

Figure 5 shows the measured poly-gate field transistor characteristics, which is the worst case for parasitic device operation because the poly-gate field transistors have a much lower threshold voltage than do the metal-gate field transistors due to a relatively thinner oxide thickness. As can be seen in this graph, the p-field transistor has good isolation characteristics but the n-field transistor shows rather weak isolation characteristics. Nevertheless, these leakage current levels are still low enough that they should not cause any circuit malfunctions because even when the gate voltage is raised to 10V, the leakage current is still less than 1μA. We compared these field transistors with those fabricated from an old run and have not yet found any reasons for the relatively lower thresholds. Table 3 compares some of the process parameters which determine the threshold voltage of the n-field poly-gate transistor, while Table 4 summarizes the process and device parameters measured in this present run.

Punch-Through Voltage Test

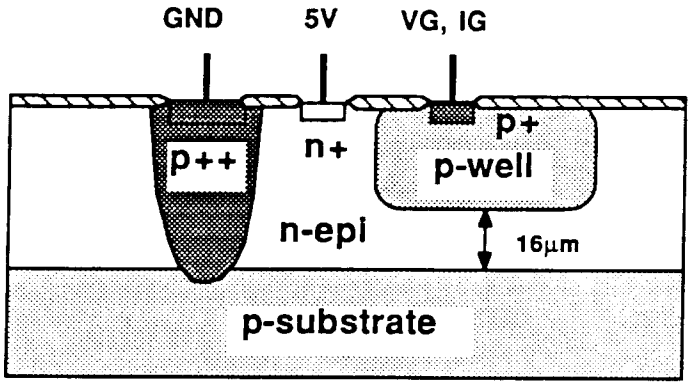

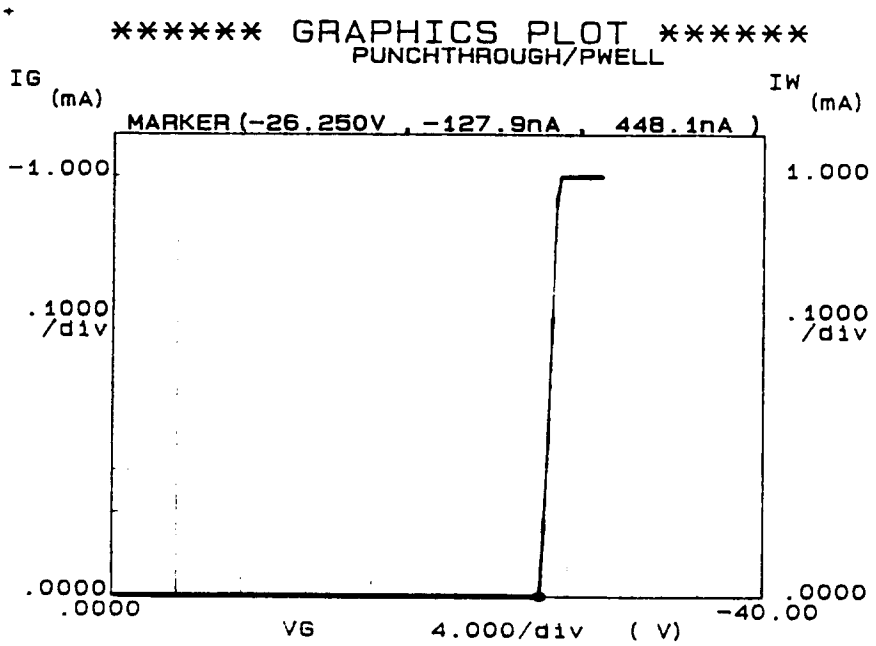

Fig. 4: Measured p-well-to-substrate punch-through characteristics. The p-substrate is biased to ground, the n-epi layer is biased at Vcc (5V), and the p-well is swept from 0V to -30V.

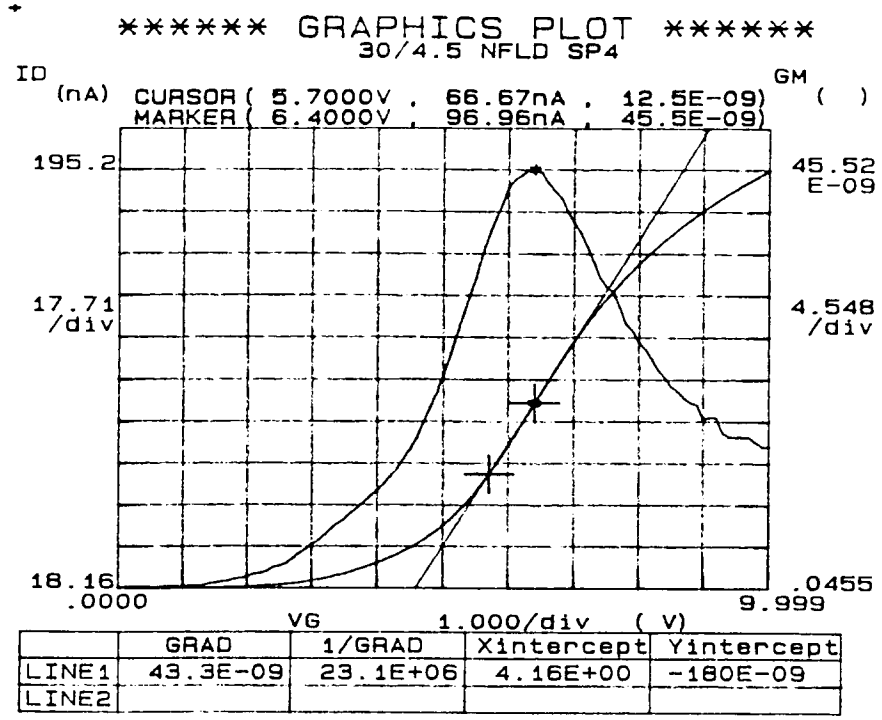

	GRAD	1/GRAD	Xintercept	Yintercept
LINE1	43.3E-09	23.1E+06	4.16E+00	-180E-09
LINE2				

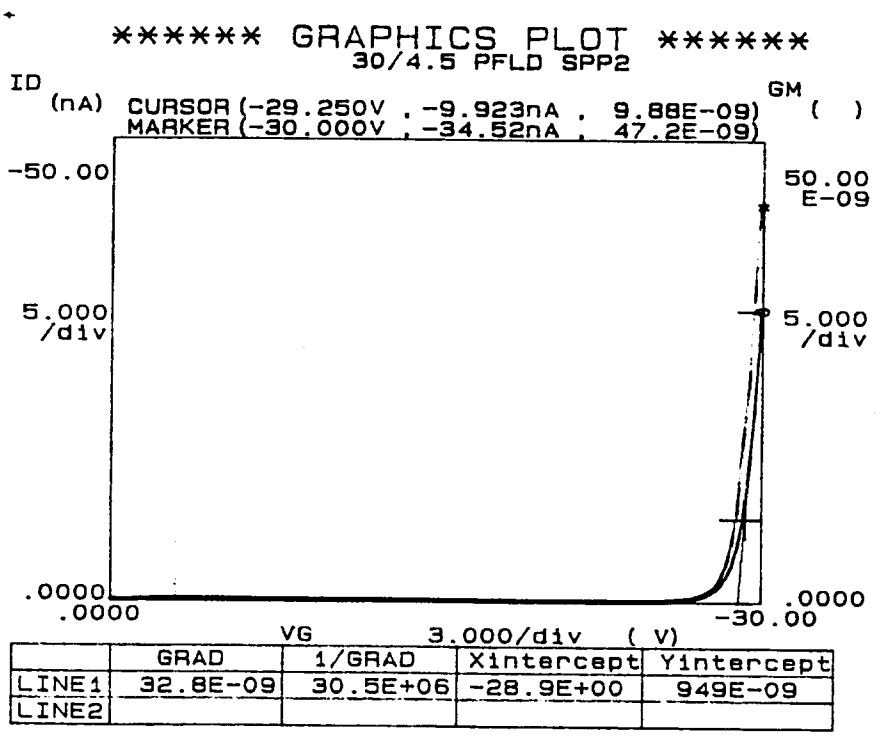

	GRAD	1/GRAD	Xintercept	Yintercept
LINE1	32.8E-09	30.5E+06	-28.9E+00	949E-09
LINE2				

Fig. 5: Measured poly-gate field transistor characteristics; (a) n-field and (b) p-field transistors. In this case, the worst case is measured because the threshold voltage of a poly-gate field transistor is much lower than that of a metal-gate field transistor.

Table 3: Comparison of process parameters for an n-field poly-gate transistor .

	Oxide thickness	P-well Implant	n-field Implant	Threshold Vtg.
OLD	5400Å	2.0E13/cm^2, 150keV	2.0E13/cm^2, 60keV	9-10V
NEW	6050Å	2.0E13/cm^2, 150keV	4.0E13/cm^2, 80keV	~4.0V

Table 4: Summary of designed process/device parameters and the actual measured values.

SPICE Parameters	**n-MOS**		**p-MOS**	
	Target	**Actual**	**Target**	**Actual**
VTO (V)	0.7	0.2~0.4	-0.7	-1.3~-1.6
KP=$\mu \cdot C_{ox}$ (μA/V^2)	50.0	82.33	25.0	36.0
Tox (Å)	300	340	300	340
GAMMA ($\sqrt{V}$)	0.98	0.917	0.40	0.189
LAMBDA (1/V)	0.025	0.0608	0.100	0.111
Field (poly) VTO (V)	>10	~4.0	>-10	~-28.9
Parameters	**Design**		**Actual**	
R sheet (n+) (Ω/sq.)	30.0		49.0	
R sheet (p+)	80.0		65.7	
R sheet (p-well)	3.36K		2.45K	
R sheet (poly)	20.0		18.3	
p-well punch (V)	>10		26.25	
p-well-to-sub punch	>10		26.25	

As can be seen from Table 3, most of the process parameters are in a reasonable range. However, the actual threshold voltages of the CMOS devices are somewhat off of their design targets. Fortunately, most of the circuitry in STIM-2 is digital and was designed to handle these parameter shifts without adverse effects. Any DAC current shifts can be easily corrected by adjusting the positive and negative supply voltages.

CIRCUIT LEVEL TESTS

STIM Circuits

Using an HP 8016 word generator, serial clock and data inputs can be generated for the STIM-1 and STIM-2 circuits. These inputs are converted into actual clock and data signals (tri-level signals at Vcc, Gnd, and Vss) for the STIM chips (STIM-1B, STIM-1A, and STIM-2) by customized tri-state buffers. The operating frequency for clock and data inputs can be adjusted using the word generator frequency setting. Test results show that all of the probe circuits operate as designed. Figures 6 and 7 show photomicrographs of the circuit portions of the active probes STIM-1B, STIM-1A, and STIM-2. The flexible interconnects used in one version of STIM-2 to obtain a low-profile chronic probe are shown in Fig. 7. As noted in an earlier report, the circuit portion of this probe can fold flat onto the cortex to minimize the height of the probe above the cortical surface and allow the dura to be replaced over the implant site. This should minimize tissue overgrowth and possible anchoring of the probe to the skull. Table 5 summarizes the specifications for the active stimulating probes fabricated in this run.

Table 5: Specifications for the active stimulating probes.

Feature	**Monopolar (STIM1B)**	**Bipolar (STIM1A)**	**Fully Parallel (STIM2)**
# Simultaneously Active Channels	1	2	8
Voltage supplies	±2.5 to ±5V	±5V	±5V
Current Source	Off-Chip	On-Chip	On-Chip
• Range (μA)	Off-Chip	±254	±127
• Resolution (μA)	Off-Chip	2	1
Transistor Count	400	1400	5000
No. of Shanks	2	8	8 (16)
No. of Sites	16	16	64
Circuit Area (mm^2)	0.8	2.6	11.2

STIM-1B

STIM-1B is the monopolar version of the active stimulating probe. In this case, site address information is entered serially using the clock to increment an on-chip counter. The counter state is decoded to select the desired site, which receives the externally-generated current via an on-chip multiplexer. Figure 8 shows the operation of the monopolar probe. The upper trace is the input clock signal, which is used to set the site address. The address here is set first at site #8 and is then switched to site #7. The middle trace shows the site drive signal, which in this case is an arbitrary waveform used for illustration only. The bottom trace shows the measured voltage output waveform at site #7. The reason for the slow falling output waveform when the negative reset clock appears is due to the high impedance of the test condition. Site #7 receives input only when addressed.

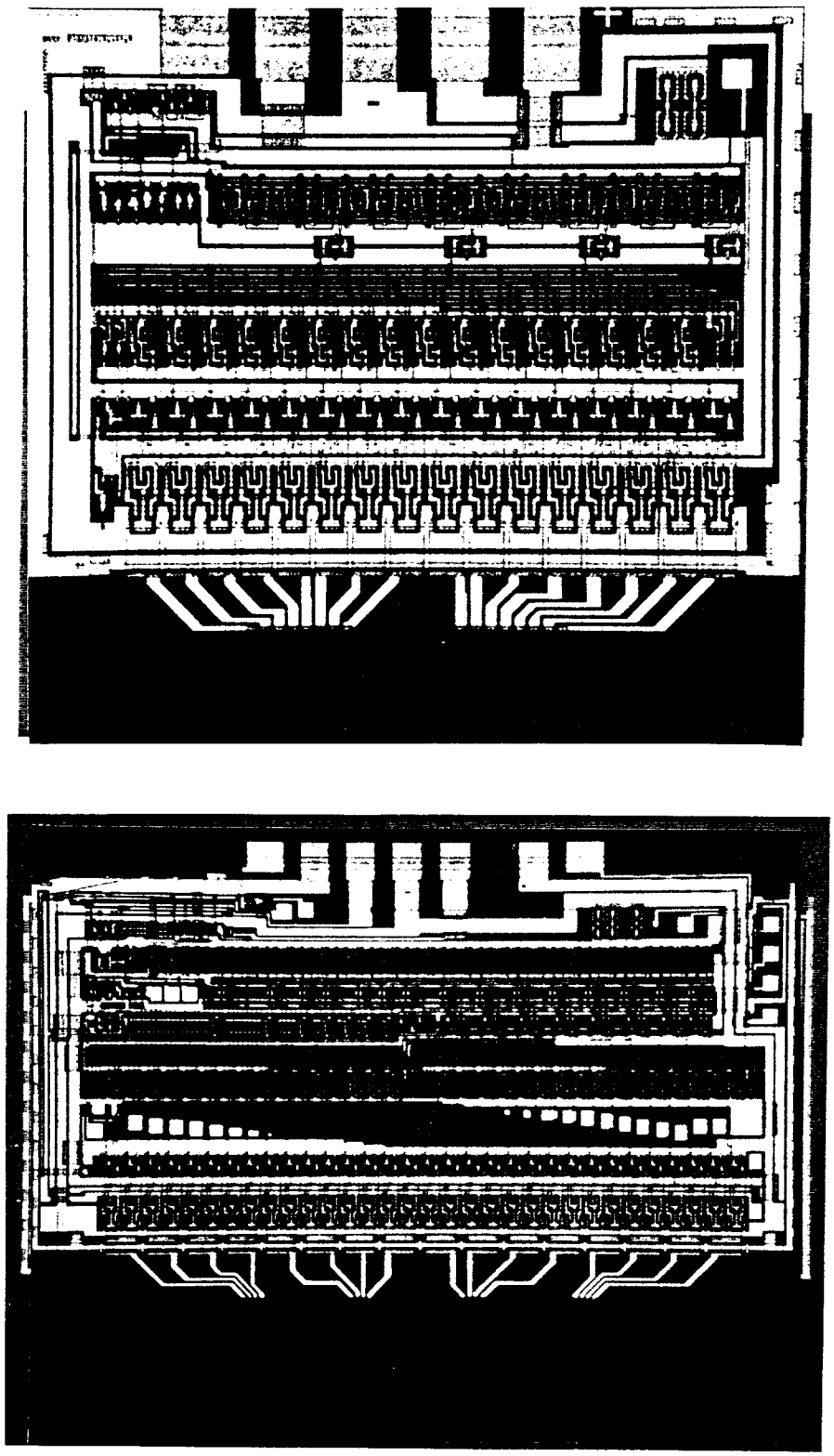

Fig. 6: Photomicrographs of the circuit portions of the active probes fabricated in this run: (above) STIM-1B, and (below) STIM-1A.

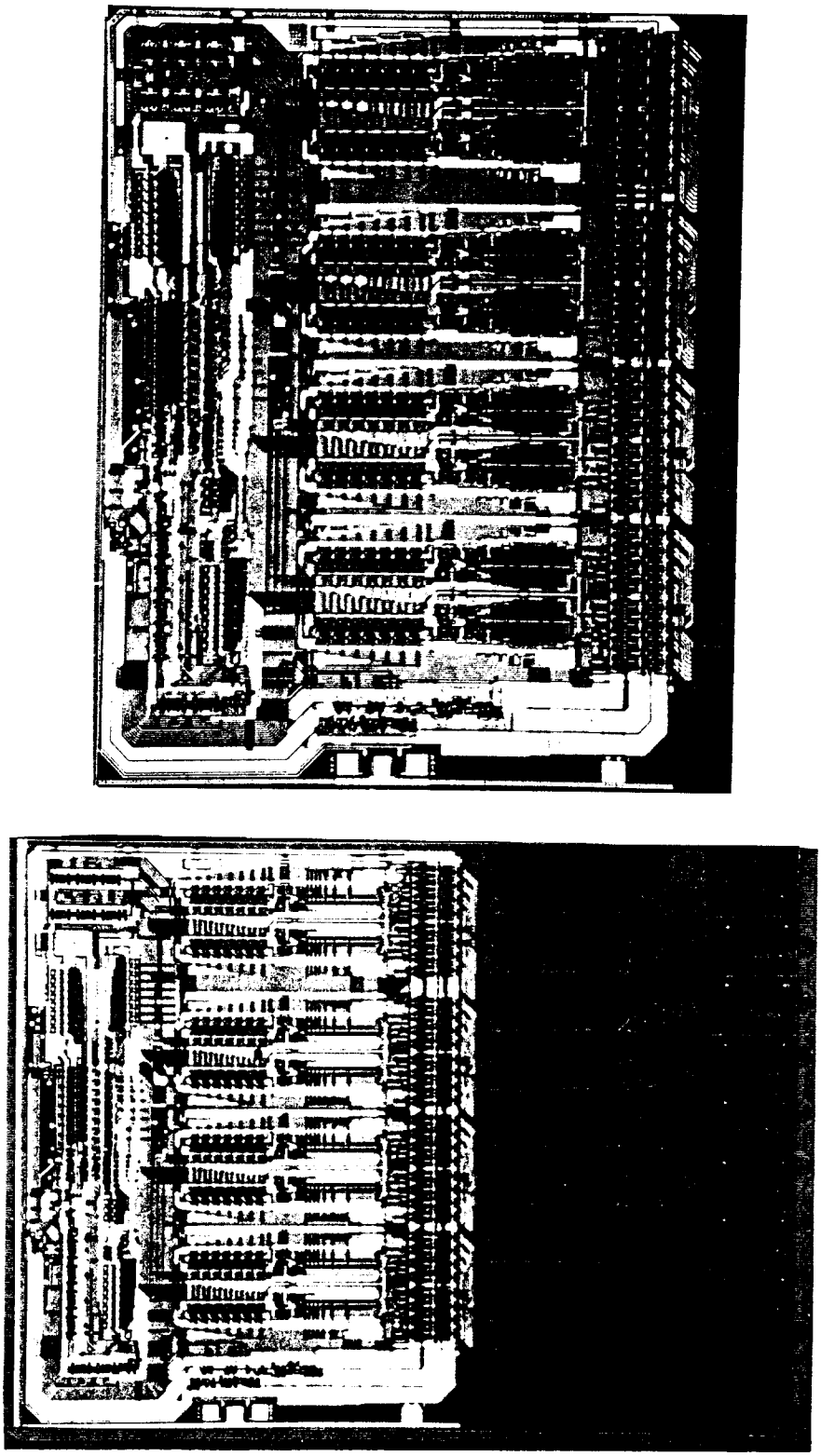

Fig. 7: Photomicrographs of the circuit portions of a STIM-2 active probe fabricated in this run. The bottom photograph shows flexible interconnects for the low-profile version of this active probe.

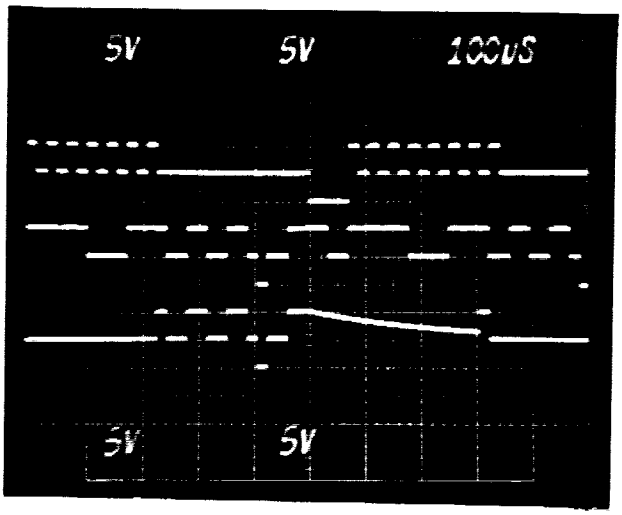

Fig. 8: Operation of the monopolar probe. Upper trace: input clock signal; middle trace: site drive signal, which in this case is an arbitrary waveform used for illustration only; bottom trace: measured voltage output waveform. Site #7 receives input only when addressed.

STIM-1A

STIM-1A is a medium complexity version of the stimulating probes which is used for a bipolar applications. To effectively stimulate the tissue, a bipolar current drive scheme is adopted; both current sourcing and sinking operations are possible simultaneously on the sites during an active cycle. In the bipolar case, eight bits of serial data are used to select two sites. The subsequent 8 bits of current amplitude data are then used on-chip to generate the stimulus current for the first site using a current-output digital-to-analog converter (DAC). This current is mirrored to the second site to form a bipolar pair.

Figure 9 shows the operation of the bipolar probe. The upper traces are the 16 input clock cycles that are used to control the shift register, which accepts external data information. The center trace shows the site-drive data signals (address and current level). The address here is set first at site #16 to generate the maximum sink current and is then switched to provide the maximum sourcing current. The bottom trace shows the measured voltage output waveform at site 16 across a 10kΩ resistor. Site #16 properly provides the maximum sourcing and sinking current alternatively when addressed.

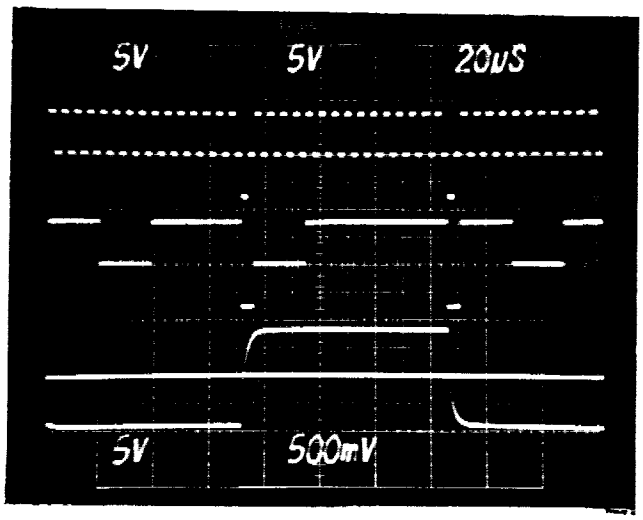

Fig. 9: Operation of the bipolar probe. The top trace is the 16-cycle input clock and the middle trace shows the input address and current level data. In this case, site #16 is selected and full scale current is provided both sourcing and sinking. The bottom trace shows the measured voltage output waveform at site #16 across a 10kΩ resistor.

STIM-2

STIM2 is a second-generation probe that significantly extends the first-generation design in a number of areas: 1) flexible interconnects, fabricated as part of the chip, allow the rear portion of the circuit area to be folded flat against the cortical surface to reduce the probe height above the cortex to <1mm, which results in a low-profile probe; 2) the probe offers a variety of new circuit designs to reduce power and circuit area while increasing functionality; 3) a front-end channel selector allows any 8 of the 64 sites to be driven simultaneously, effectively implementing electronic site positioning; and 4) the probe is directly compatible with use in multi-probe three-dimensional arrays, initially targeted at 256 shanks and 1024 sites. The following measurements have been performed on the STIM-2 circuitry.

The stimulating electrode sites are driven by an 8-bit CMOS DAC. It is controlled by a seven-bit channel latch which controls a string of current mirrors. During the normal active cycle, the CP clock selects either the p-DAC (CP=1) or the n-DAC (CP=0). A total reference current of only 1μA flows to control a whole string of current mirrors, resulting in a small layout area and low power consumption. The current levels of the transistors are designed to double at each successive stage by using the same unit transistor, preserving current linearity regardless of power supply voltages and process parameters. This power-efficient DAC is designed to deliver bipolar currents ranging from -127μA to +127μA with 1μA resolution. Figure 10 shows DAC operation.

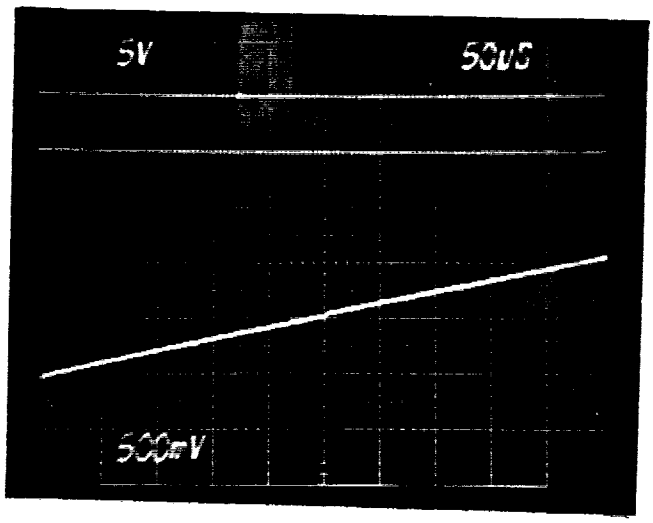

Fig. 10: DAC operation when the input is cycled over its full range of current levels. The top trace is the input clock and the bottom trace is the voltage waveform across a 20kΩ resistor.

The power-on-reset (POR) comes up in the correct state in order to reset the initial conditions when the Vcc supply voltage is turned on. In this state, the sites are connected to the data pad for analog access to the sites during activation. The first positive clock pulse resets the POR circuit correctly. Figure 11 shows the waveforms for POR clock operations. The POR signal is generated by the positive power supply, Vcc, and goes to ground level when the first clock comes in, remaining low during subsequent operating cycles due to the latching type of circuit configuration used.

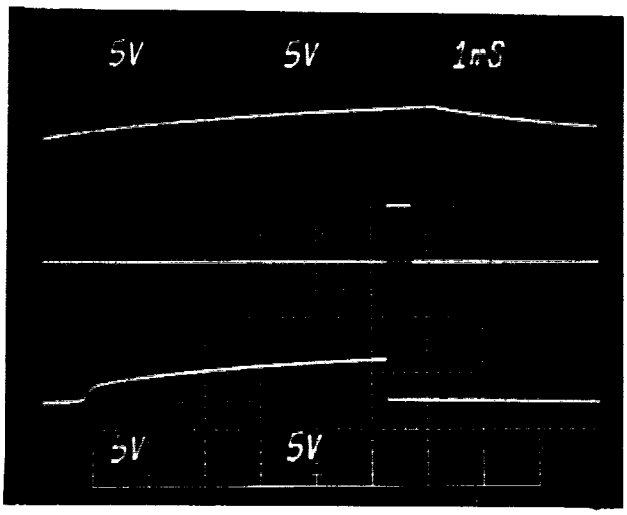

Fig. 11: POR clock operation when Vcc power is up and the first clock comes in. The top trace is the Vcc power supply voltage, the center trace is input clock, and the bottom trace is the POR clock.

Figure 12 shows negative pulse detector operation as used for the CST (CLOCK strobe) or DST (DATA strobe) clocks, which latch the address, mode, and current data bits derived from the external CLOCK and DATA signals. If the input levels of the control signals (CLOCK and DATA) are either Vcc or GND for normal data transfer, then the CST (or DST) clock stays at ground level (L) with no static power consumption. When the input levels go negative (Vss), however, this clock goes to a high state (Vcc) where it remains until the negative input pulse disappears; hence, control pulses are generated from the input signals as needed.

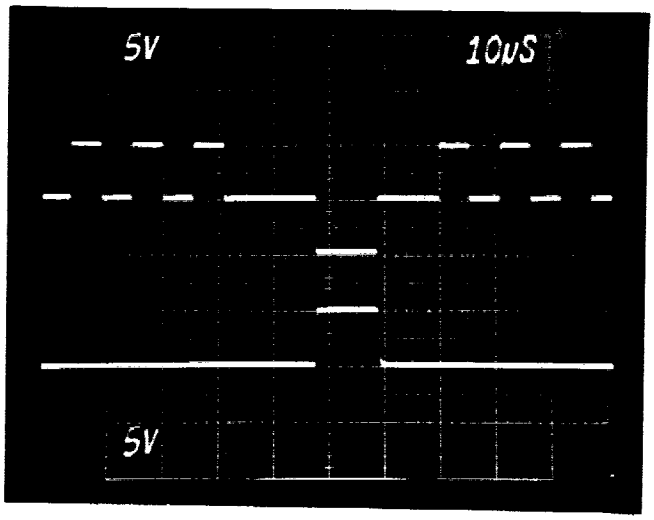

Fig. 12: Negative pulse detector operation. When the input signal goes to a negative value, a clock is generated which latches the address, mode, and current data.

The level-shifter operates properly and converts standard CMOS input signals (Vcc (5V) and GND (0V)) to appropriate inputs for the DAC (Vcc (5V) to Vss (-5V)) as shown in Fig. 13.

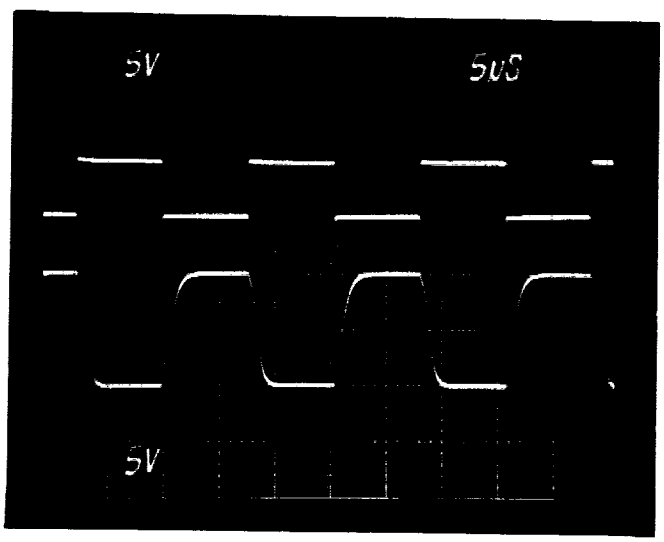

Fig. 13: Test results showing level-shifter operation. The top trace is the input clock (Vcc to Gnd) and the bottom trace is its output waveform (Vcc to Vss).

The shift register accepts data serially under control of the clock. Figure 14 shows the output of the shift resister during clocking. In this case, output 0 (SH000) and output 7 (SH111) are selected. After 8 clock cycles, the SH000 output stays low and the SH111 output remains high according to the input data.

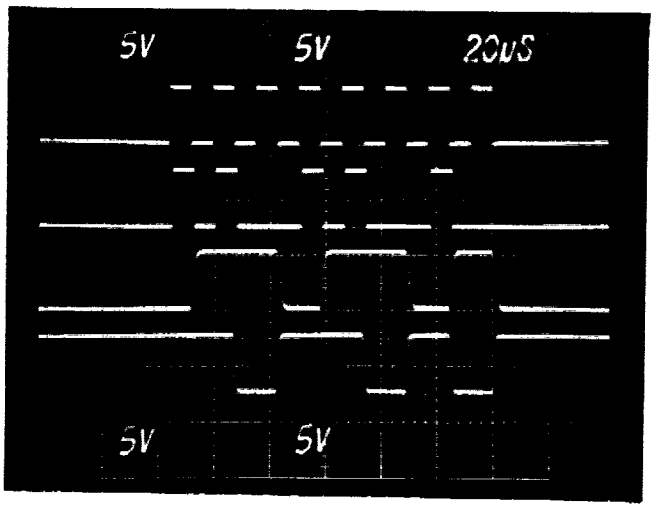

Fig. 14: Output of the shift register during clocking. In this test, output 0 (SH000) and output 7 (SH111) are selected. Top trace is the control clock, the second trace is arbitrary data information, and the third and fourth traces are the outputs SH000 and SH111, respectively.

The address and mode latches at the output of the shift-register latch onto the data when strobed by a negative pulse on the data line (DST clock), and the address and mode decoders properly decode the address and mode state and enable the appropriate channel. Figure 15 shows an address decoder output of DEC24 (DAC decoder for #4). During the falling edge of the DST clock, the actual address is latched. In this test, DAC4 is selected.

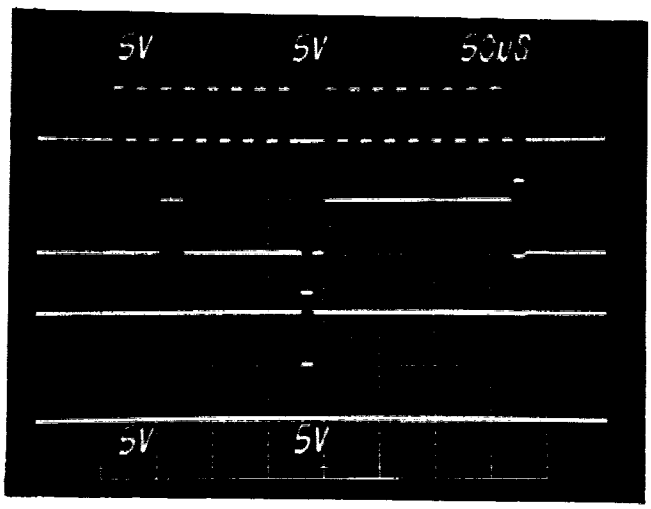

Fig. 15: Address decoder output of DEC24 (DAC decoder for #4) when addressed. The top trace is the input clock, the second trace is the input data information, and the third and forth traces are selected (DEC24) and unselected (DEC27) decoder outputs, respectively.

The addressed per-channel data latches lock onto the data when the clock line is strobed negatively, and the DAC generates the appropriate currents. Figure 16 shows the output voltage waveforms across a 20kΩ resistor load when the current level data alternates from (0111111) to (1111111) for a sourcing case (CP=1).

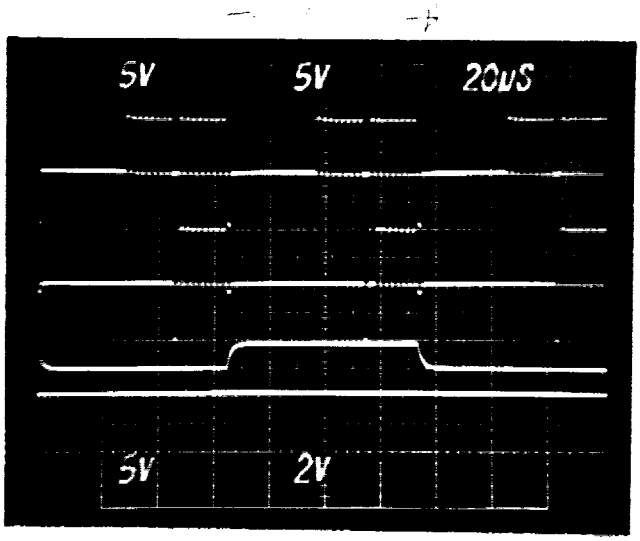

Fig. 16: Output voltage waveforms across a 20kΩ resistor load when the current level data alternates from (0111111) to (1111111) in the sourcing mode (CP=1).

Probe Edge Optimization

As mentioned in earlier quarterly reports, it is important to retain a wide boron-doped boundary layer around the circuit areas of the active probes in order to avoid excessive undercutting during the final separation etch in EDP. This was a significant problem in the first runs of STIM-1, especially near the corner regions. The problem arises due to the fast etching rates in silicon along the <100> directions, which are typically at 45° to the major probe edges if a rectangular geometry is used. The slowest etching rate is usually achieved in <111> directions. In the design of STIM-2, we have used rounded corners on the probe to help guard against irritation of the tissue and have used a much wider heavily boron-doped silicon boundary region (≥190μm) than that of STIM-1 (~100μm) to minimize the chance of undercutting into the circuit area. However, an additional problem has been recognized in connection with the formation of active probes containing silicon ribbon cables as in the low-profile version of STIM-2. If the probe shanks or the ribbons are aligned with the major wafer flat (i.e., along the <110> direction), then the etch will not undercut the shank/ribbon from the front but will instead "V" into the open areas on either side of it. The sides of the "V" correspond to the <111> silicon planes and will not undercut. When the etch from the back reaches the bottom of these areas, it will rapidly etch laterally under the shank/ribbon, but in order to etch down to the appropriate thickness, especially on a thin ribbon, requires that the etch virtually etch the lightly-doped circuit area away. This problem was not recognized earlier and resulted in the loss of virtually an entire run of STIM-2 since it is common practice to align the probes to the major wafer flat.

On the last run of STIM-2, we deliberately aligned the masks at 22° off the major flat so that undercutting would occur along the shank/ribbon from the front, eliminating the problem. For a shank or ribbon cable 75μm wide and 500μm long, it is only necessary to align about 8.5° off the major flat to ensure undercutting from the front. The 22° misalignment used here resulted in adequate undercutting but also produced rather uneven edges on the probe circuit areas as the etch attempted to conform to the major crystallographic directions. Dropping the alignment angle to around 10° should reduce this problem and yield probes whose edges are effectively smooth while preserving the ability to undercut critical shank/ribbon areas from the front and providing adequate protection to the circuit areas. The yield of low-profile probes has been very high with no significant problems encountered in handling. This is the first time that a probe of this sort (using ribbon cables to join two thicker areas) has been fabricated. The rear circuit areas bend at right angles to the shanks quite readily.

4. Conclusions

During the past quarter, research under this program has gone forward in a number of areas. Passive probe fabrication has continued with the fabrication of several runs of "EMORY" probes. A set of "HMRI" probes are also ready for metal. Problems with our iridium target, which separated from its backing plate recently, have been fixed and a backup iridium target has been ordered to avoid any problems in the future. Probes for studies of tissue penetration, aimed at quantifying the insertion force required for pia arachnoid and dura mater as a function of tip shape, are nearing completion along with a workstation-based system for data acquisition and analysis. These probes feature a wide range of tip angles and shapes, fabricated both with single- and with double-diffused processing. Initial tests of these probes are expected during the coming term. Studies of chronic stimulating electrode impedance and tissue access voltage are underway as well, and while only preliminary results are available at this writing, impedances have been observed to generally increase during stimulation but to decline over time between stimulation sessions. The access voltage drops significantly after several days of stimulation. These studies are continuing and more conclusive results should be available during the coming quarter.

A fabrication run of second-generation active stimulating probes has been completed through circuit metallization. Test results have shown small deviations in the threshold voltages from the design targets and a low poly-gate field transistor threshold; however, transistor leakage currents are nonetheless submicroampere over the expected operating range of the circuitry. Significant leakage problems associated with earlier active probes have been eliminated by using wider p-well-to-p-well separations and a wider epitaxial layer. Tests have shown that all of the STIM-1B (monopolar), STIM-1A (bipolar), and STIM-2 (8 of 64 parallel) circuit blocks are fully functional, with performance near design targets. This includes the functions of power-on-reset, internal clock generation, data input, data latching, channel selection, level shifting, and digital-to-analog conversion. These probes are now being completed with the application of LTO over the circuit areas, the addition of iridium at the sites, and the use of micromachining to free them from the wafer. We hope to have fully functional probes during the coming quarter.

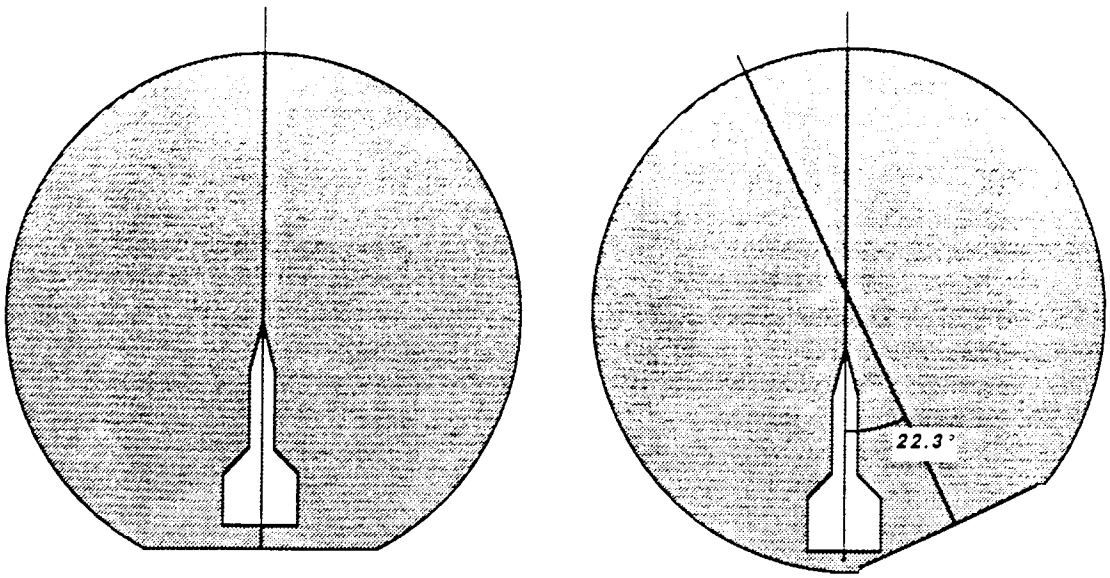

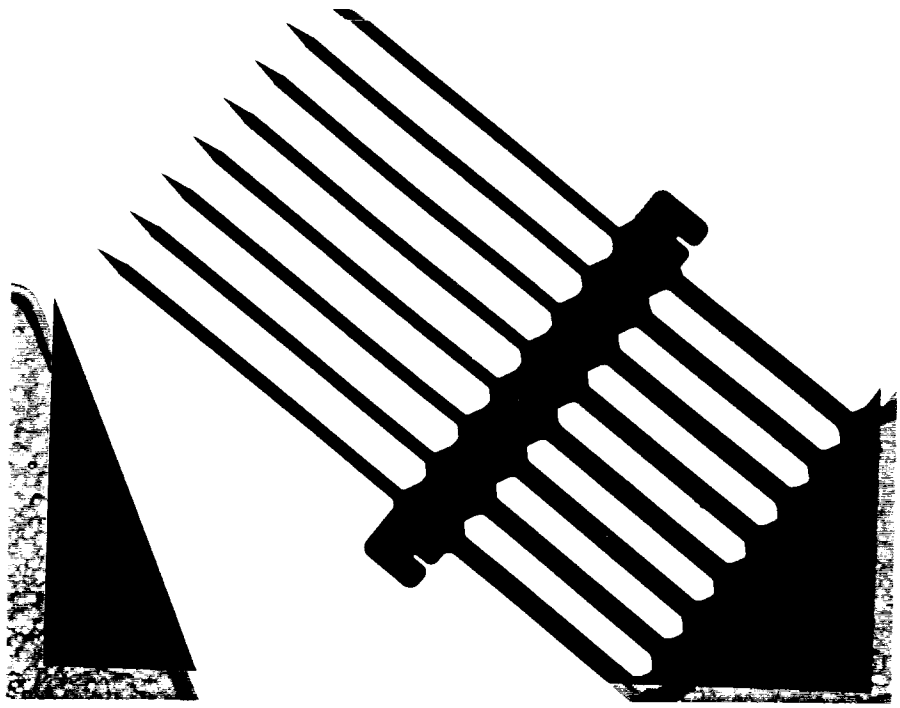

Fig. 17: Test results on an etched active probe after die separation when the probe mask was aligned at an angle of 22.3° from the major <110> wafer flat.